doi:10.26443/seismica.v3i2.1375

Insolation Cycles Control the Timing and Pattern of Resonance Frequency Drifts at a Natural Rock Tower, Utah, USA

Jeffrey R. Moore * [1], **Erin K. Jensen** [1], **Brendon J. Quirk** [1], **Guglielmo Grechi** [1,2], **Alex Dzubay** [1]

[1]Department of Geology and Geophysics, University of Utah, Salt Lake City, UT, USA, [2]Department of Earth Sciences, Sapienza University of Rome, Rome, Italy

Author contributions: *Conceptualization* J.R. Moore, E.K. Jensen, B.J. Quirk. *Formal Analysis* J.R. Moore, E.K. Jensen, B.J. Quirk, G. Grechi. *Funding Acquisition* J.R. Moore, E.K. Jensen. *Investigation* J.R. Moore, A. Dzubay. *Writing – original draft* J.R. Moore, E.K. Jensen, B.J. Quirk, G. Grechi, A. Dzubay. *Writing – review & editing* J.R. Moore, E.K. Jensen, B.J. Quirk, G. Grechi, A. Dzubay.

Abstract Resonance frequency monitoring can detect structural changes during progressive rock slope failure; however, reversible environmentally driven frequency drifts may inhibit identification of permanent changes. Frequency drifts are commonly correlated with air temperature, lagging temperature changes by zero to 35–60 days. Here we report observations from two years of monitoring at a rock tower in Utah, USA where annual resonance frequency changes appear to precede air temperature cycles by approximately 35 days. Using correlations with meteorological data supplemented by numerical modeling, we identify changes in insolation as the primary driver of annual frequency drifts, giving rise to the observed negative lag time. Sparse in-situ insolation data show that the daily resonance frequency increase lags sunrise by several hours, while frequencies decrease at sunset, responses we attribute to the west facing aspect of the tower. Modeled daily insolation corresponds with frequency data for months when measurements are not available. Numerical models offer the advantage of predicting insolation patterns for different aspects of the rock tower, such as the west facing cliff where measurements would be challenging. Our study highlights the value of long-term datasets in identifying mechanisms driving environmentally associated frequency drifts, understanding that is crucial to facilitate detection of permanent changes during progressive failure.

Production Editor: Théa Ragon
Handling Editor: Pablo Heresi
Copy & Layout Editor: Anant Hariharan

Signed reviewer(s): Sebastiano D'Amico

Received: May 7, 2024
Accepted: October 22, 2024
Published: November 22, 2024

1 Introduction

Analyses of in-situ ambient vibration data are becoming increasingly utilized in slope stability monitoring (Jongmans et al., 2015; Bottelin et al., 2021; Colombero et al., 2021b; Jensen et al., 2024). Important past studies have established critical groundwork, showing for example that: a) the dynamic properties (i.e., resonance frequencies, damping ratios and mode shapes) of unstable rock slopes can be determined from ambient seismic data (Burjánek et al., 2010, 2012; Del Gaudio and Wasowski, 2011; Bottelin et al., 2013a; Valentin et al., 2017; Moore et al., 2019; Finzi et al., 2020; Dzubay et al., 2022; Müller and Burjánek, 2023); b) in-situ vibration measurements can be used to describe the structural conditions of rock slope instabilities (Moore et al., 2011; Pilz et al., 2014; Colombero et al., 2017, 2021b; Del Gaudio et al., 2013; Valentin et al., 2017; Kleinbrod et al., 2019; Häusler et al., 2019, 2021; Bessette-Kirton et al., 2022); and c) resonance frequencies of an unstable rock mass change during progressive slope failure and/or slope remediation, indicating their potential as a valuable monitoring metric (Lévy et al., 2010; Bottelin et al., 2017; Burjánek et al., 2018; Fiolleau et al., 2020; Colombero et al., 2021a; Taruselli et al., 2021; Jensen and Moore, 2023). Meanwhile, in-situ vibration measurement technology has advanced at a rapid rate; seismic sensors are smaller, cheaper, and more robust, with new low-cost instruments enabling increasingly diverse applications (Anthony et al., 2019; Bottelin et al., 2021; Arosio et al., 2023).

Apart from permanent frequency shifts, cyclic frequency variations driven by environmental effects can be large (1–30% of average) and have the potential to mask irreversible changes related to stability (e.g. Bottelin et al., 2021; Colombero et al., 2021b; Jensen et al., 2024). Frequency changes are often positively correlated with temperature because of increased grain contact stresses and the closure of micro and macrocracks during thermal expansion, both of which cause corresponding increases in material and fracture stiffness (Bottelin et al., 2013b; Starr et al., 2015; Colombero et al., 2021b; Geimer et al., 2022). Past studies have shown that on an annual or seasonal scale, resonance frequencies can respond immediately (with no time delay) to air temperature changes (Colombero et al., 2017; Burjánek et al., 2018; Geimer et al., 2022; Jensen et al., 2024). Otherwise, the annual frequency response can lag air temperatures (i.e., frequency is directly correlated with air temperature from a certain number of days in the past) by $\sim$ 35 to 60 days (Bottelin et al., 2013b; Colombero

*Corresponding author: jeff.moore@utah.edu

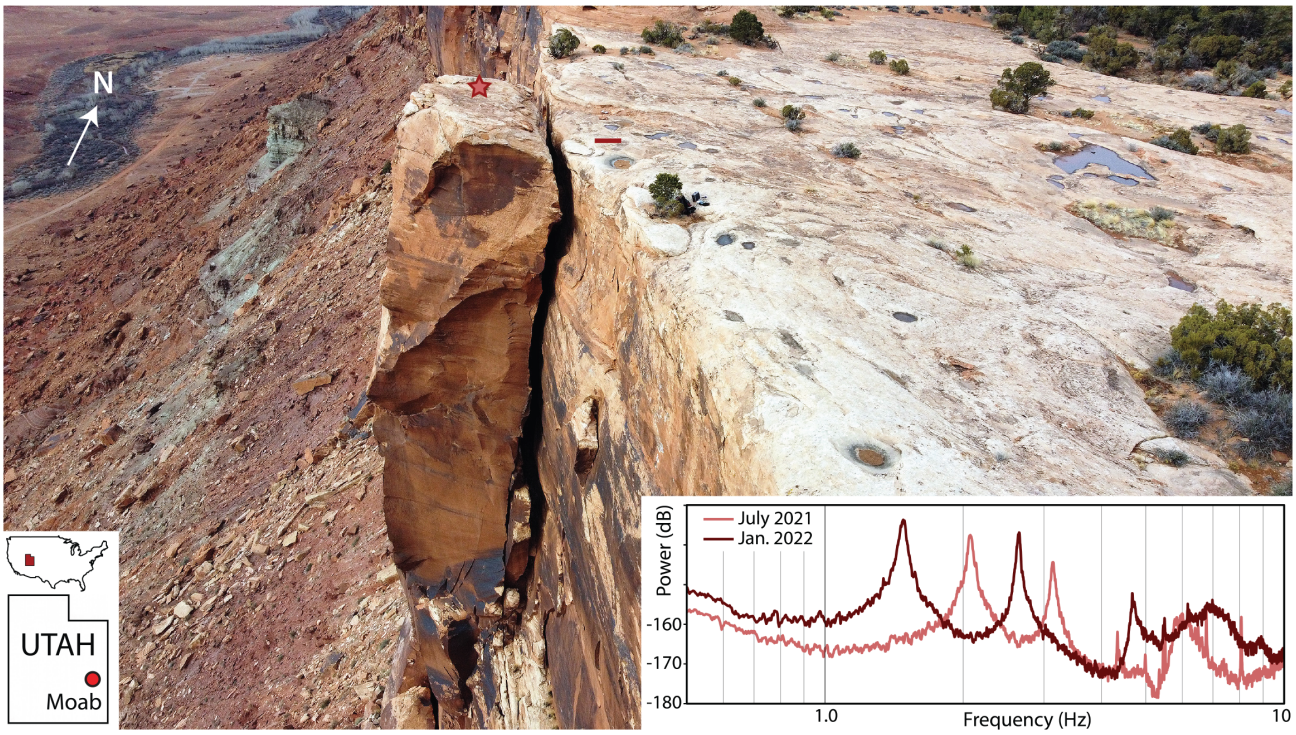

Figure 1 Aerial view of Kane Springs Tower, located near Moab, Utah. The rear crack separating the tower from the cliff is open (0.5–1 m aperture) to a depth of 20 m. Star shows location of the seismometer, red bar is $\sim$ 1m scale. Inset BHE spectra from July 1, 2021 and January 1, 2022 show clear frequency peaks for the first two modes of the tower and their annual drift. Decibel power is relative to 1 m^2 s^{-2} Hz^{-1}.

et al., 2021b). In such cases, thermal diffusion and corresponding delays in the opening and closing of fractures are primarily attributed to temperature-frequency delays (Colombero et al., 2021b). Alternatively, stress changes from differential dilation between the surface and interior of the bulk rock mass have also been observed to drive an immediate frequency response to air temperature even when fracture opening is lagged with temperature (Jensen et al., 2024). On a daily scale, hourly data comparisons have revealed delays between frequency and air temperature ranging from 0 to 23 hours (Colombero et al., 2021b). In addition to the relevance of thermal diffusion on a daily scale, the relative influences of radiative and convective heat fluxes and the site's orientation relative to the sun have also been recognized as important factors driving the relation between frequency and air temperature (Guillemot et al., 2022, 2024).

Here we describe a new ambient vibration dataset used to monitor resonance frequencies over two years at a 36-m high freestanding sandstone tower in Utah, USA. Interestingly, while most past datasets, including some from the same region (Geimer et al., 2022; Jensen et al., 2024), show that frequencies are either in phase with or lag changes in air temperature, our data exhibit a different trend where frequency changes appear to precede air temperature changes. More specifically, our data demonstrate that resonance frequencies are directly correlated with the annual pattern of insolation, which we confirm through analysis of regional meteorological data and numerical modeling. Sparse in-situ insolation data and model results additionally show that resonance frequencies of the tower follow daily solar radiation trends, specifically insolation predicted for the west-southwest facing tower cliff. Our measurements offer important new understanding of environmentally driven resonance frequency drifts, highlighting the value of long-term monitoring datasets and aiding efforts to use resonance monitoring in slope stability analysis and failure prediction.

2 Site Description

Kane Springs Tower (Figure 1) is an approximately 36-m high freestanding rock tower located 17 km southwest of Moab, Utah, composed of massive Jurassic Wingate Sandstone. It is approximately 5 m wide and 13 m across. The tower formed through partial collapse of a slab from the NW-trending (330°) cliff face. The crack separating the tower from the adjoining cliff is 0.5–1 m wide at maximum and extends to a depth of 20 m where it fills with rubble. We instrumented Kane Springs Tower with a single Nanometrics Trillium Compact 20-s seismometer recording continuous data at 50 Hz between 20 Feb, 2021 and 21 Feb, 2023, with some data gaps and days of partial coverage caused by a malfunctioning battery. The seismometer was aligned to north, leveled, and adhered to the bedrock surface using silicone glue, before being covered with an insulated plastic bucket that was similarly glued to the rock. Modal analysis of the tower was previously presented by Dzubay et al. (2022), who used translational and rotational seismometer data, together with numerical modeling, to describe resonance frequencies, damping ra-

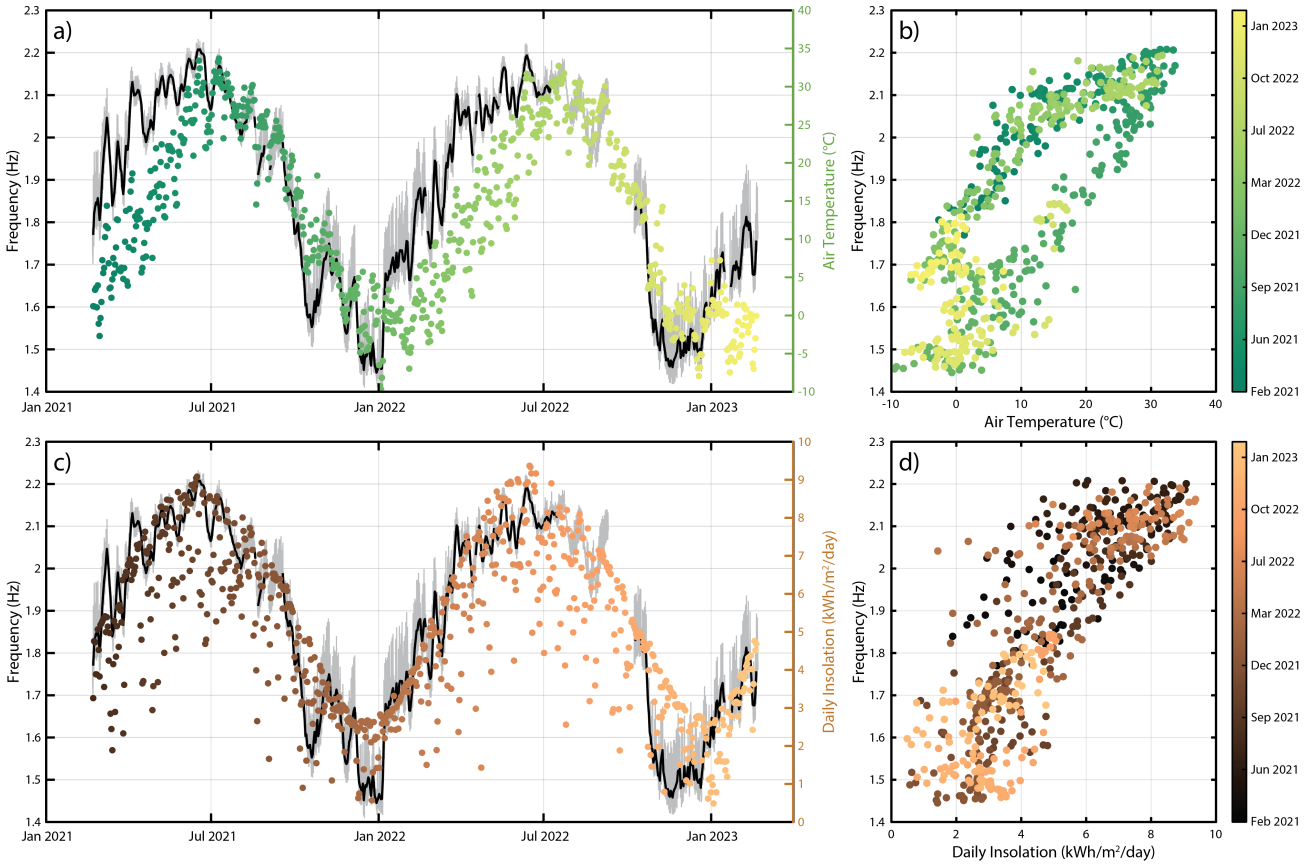

Figure 2 (a) First resonance frequency of Kane Springs Tower and air temperature measured at station KCNY; temperature is colored by date. Daily average frequencies are shown in black, original 30 min data in gray. (b) First resonance frequency plotted against air temperature. Data indicate a negative lag where frequency changes precede temperature; best fit can be achieved by a -35 day lag. (c) First resonance frequency of Kane Springs Tower and daily insolation measured at Flattop Mountain; insolation is colored by date. (d) First resonance frequency plotted against daily insolation. Data reveal in-phase correlation with no apparent lag.

tios and mode shapes for the first six resonance modes. The first two modes of the tower were found to be bending against the thinner and thicker horizontal dimensions, respectively, while the third mode is torsion about a vertical axis. Previous site-to-reference measurements additionally confirmed that resonance frequencies measured on the tower were not measured on the adjoining mesa $\sim$ 50 m away. Dzubay et al. (2022) also presented a portion of the monitoring data, showing frequency drifts over the first year in order to link measurements made by different instruments at different times, but they did not analyze the cause of these drifts.

3 Datasets and Methods

We processed continuous ambient vibration data from the seismometer installed on Kane Springs Tower (station code: KSLTA) for spectral attributes in order to identify and track resonance frequencies over time. All seismic data were de-meaned, de-trended, instrument-response-corrected, and band-pass filtered between 0.1–10 Hz to analyze relevant velocity data in m/s. We computed the power spectral density (PSD) for each component by calculating fast Fourier transforms of 60-s Hanning-tapered windows with 50% overlap, and averaged the PSD to reduce variance (Koper and Burlacu, 2015). Following methods described by Geimer et al. (2022) and Jensen et al. (2024), we used the Random Decrement Technique (RDT) (Cole Jr, 1973; Ibrahim, 1977) to track resonance frequencies in 30-minute intervals over the monitoring period. We used the BHE (east-west) component to track modes 1 and 2, which are clearly identifiable in spectra from monitoring data; we did not attempt to track higher-order modes as these are not consistently clear over time given the station location.

We recorded in-situ rock temperature data continuously over the monitoring period from a sensor embedded 2 cm into the rock surface on a west facing aspect of the upper part of the cliff. Later in the monitoring period, we installed a small meteorological station at the site measuring air temperature and relative humidity, as well as solar radiation. However, the radiation sensor proved extremely unreliable and recorded only 14 days of continuous data despite several repair attempts. Because we lacked air temperature and radiation data covering the entire monitoring period, we gathered additional data from available weather stations. We use the air temperature record from the Canyonlands Field weather station (KCNY; mesowest.utah.edu), 25 km northwest of Moab at a similar elevation, and solar radiation data from the Flattop Mountain weather station, 120 km northwest of Moab at a slightly higher elevation

(utFTOP; raws.dri.edu). Several months of coeval air temperature measurements from Kane Springs Tower show nearly identical readings to those from KCNY. We elected to use Flattop Mountain radiation data instead of a slightly closer station because the latter was located on a hillside, which adversely affects radiation measurements, and was at higher elevation. Insolation compared across these regional distances is intended to primarily capture seasonal changes in solar radiation, and cannot account for short term changes caused by cloudy periods since the distance to our site is comparably large.

4 Insolation Modeling

We adapted the climate modeling approach of Plummer and Phillips (2003) to calculate insolation at our site. We used a 5-meter resolution digital elevation model (Utah Auto-Correlated DEM) as the input, and calculated the clear-sky shortwave radiation at every cell of the DEM including the effects of local relief shading. Clear-sky shortwave radiation was determined using the approach of Kumar et al. (1997) as the sum of direct (I_s), diffuse (I_d), and backscattered (I_r) radiation components:

$$I_s = I_0 \times \tau_b \times cos\ i \tag{1}$$

$$\tau_b = 0.56(e^{-0.65M} + e^{-0.95M}) \tag{2}$$

$$I_d = I_0 \times \tau_d \times cos^2(\beta/2) \times sin\ \alpha \tag{3}$$

$$\tau_d = 0.271 - 0.294\tau_b \tag{4}$$

$$I_r = I_0 \times \tau_r \times r \times sin^2(\beta/2) \times sin\ \alpha \tag{5}$$

$$\tau_r = 0.271 + 0.706\tau_b \tag{6}$$

Where I_0 is the extraterrestrial intensity on a given Julian day (here the last day of every month) calculated using modern eccentricity, M is the approximate air mass, β is slope, and r is the ground surface albedo (here held constant at 0.4). The angle of incidence, i, and solar altitude, α, are defined as:

$$i = arccos[sin\ \delta_s(sin\ l \times cos\ \beta - cos\ l \times sin\ \beta \times cos\ a_w) + cos\ \delta_s \times cos\ h_s \times (cos\ l \times cos\ \beta + sin\ l \times sin\ \beta \times cos\ a_w) + cos\ \delta_s \times sin\ \beta \times sin\ a_w \times sin\ h_s] \tag{7}$$

$$\alpha = arcsin(sin\ l \times sin\ \delta_s + cos\ l \times cos\ \delta_s \times cos\ h_s) \tag{8}$$

Where, l is latitude, h_s is the hour angle, a_w is aspect, and δ_s is the solar declination, calculated using modern obliquity.

We implemented an updated relief shading algorithm following the approach of Corripio (2003), as compared to the original model of Plummer and Phillips (2003). Using the digital elevation model as input, the routine calculates a logical value for shaded (0) and unshaded (1) regions across the landscape for a given timestep, here one half hour, which directly modifies the radiation component. Taken together, our model outputs irradiance values at thirty-minute intervals at every cell in the digital elevation model for the last day of every month. These outputs include effects of local shading, slope, and aspect, allowing for analysis and comparison of the timing and intensity of insolation across the landscape including differences between broad, flat surfaces, and cliff faces like at Kane Springs Tower.

5 Results

The first and second resonance frequencies of Kane Springs Tower were clearly visible in spectra from in-situ ambient vibration data (Figure 1). These drift noticeably over the year with the highest values measured in June or July and lowest frequencies measured in December or January. Our monitoring data span two years between 20 Feb, 2021 and 21 Feb, 2023 with a data gap of intermittent measurements in fall 2022 and a few other short gaps caused by battery malfunctions. The fundamental frequency ($f1$) varies between 1.4 and 2.2 Hz and the second resonance frequency ($f2$) varies between 2.6 and 3.2 Hz; the annual amplitude of $f2$ is about 78% that of $f1$. However, the annual patterns of frequency drift for the two modes were nearly identical, therefore we concentrate on analysis of data for the fundamental mode to assess drivers of frequency drifts.

Figure 2a shows the daily average $f1$ value plotted over time and compared with daily average air temperature at station KCNY. These datasets are not in-phase, and unexpectedly, frequency changes appear to precede air temperature changes. This is clarified by plotting $f1$ against air temperature (Figure 2b), which shows a hysteretic loop indicating a phase difference between the two datasets. We assessed the lag between frequency and air temperature by first roughly aligning the time series manually, then fine tuning the fit by maximizing the linear correlation coefficient relating the two. We find a negative lag time of 35 ± 2 days best fits the datasets, i.e., frequency changes best correlate with air temperature measured ~ 35 days in the future.

We then explored correlations with insolation, using available data from the climate station at Flattop Mountain (Figure 2c). Results show that daily average fundamental frequency and daily cumulative insolation are positively correlated and in-phase with no apparent lag (Figure 2d). Insolation data, however, often exhibit short-term dips associated with cloudy periods, which are not reflected in our resonance data, either because the climate station is too far from our site to share the same cloud conditions or because daily average frequencies do not respond to rapid insolation variations. A rapid frequency drop in October 2022 may not correlate with insolation for similar reasons.

To further explore correlations between resonance frequency and insolation, we used numerical modeling to predict (cloud-free) insolation at Kane Springs Tower. We specifically evaluated insolation on the upward-facing mesa surface adjacent to the tower as well as the west-southwest facing tower cliff. Modeled insolation trends over the year compare well with data from Flattop Mountain (Figure 3a), highlighting the annual change caused by differences in solar radiation and omitting short-term changes driven by variable cloudi-

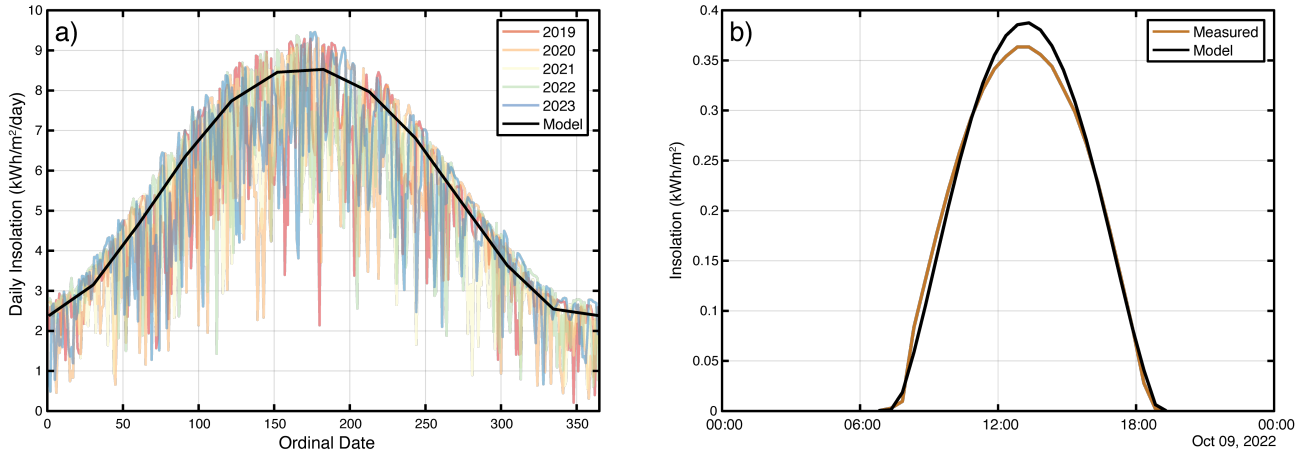

Figure 3 (a) Flattop Mountain daily insolation data for the past five years shown together with model output for the Kane Springs Tower mesa point. (b) Representative day of in-situ insolation data from Kane Springs Tower shown together with model output (mesa point) for the nearest date (Sep 30), times are MDT.

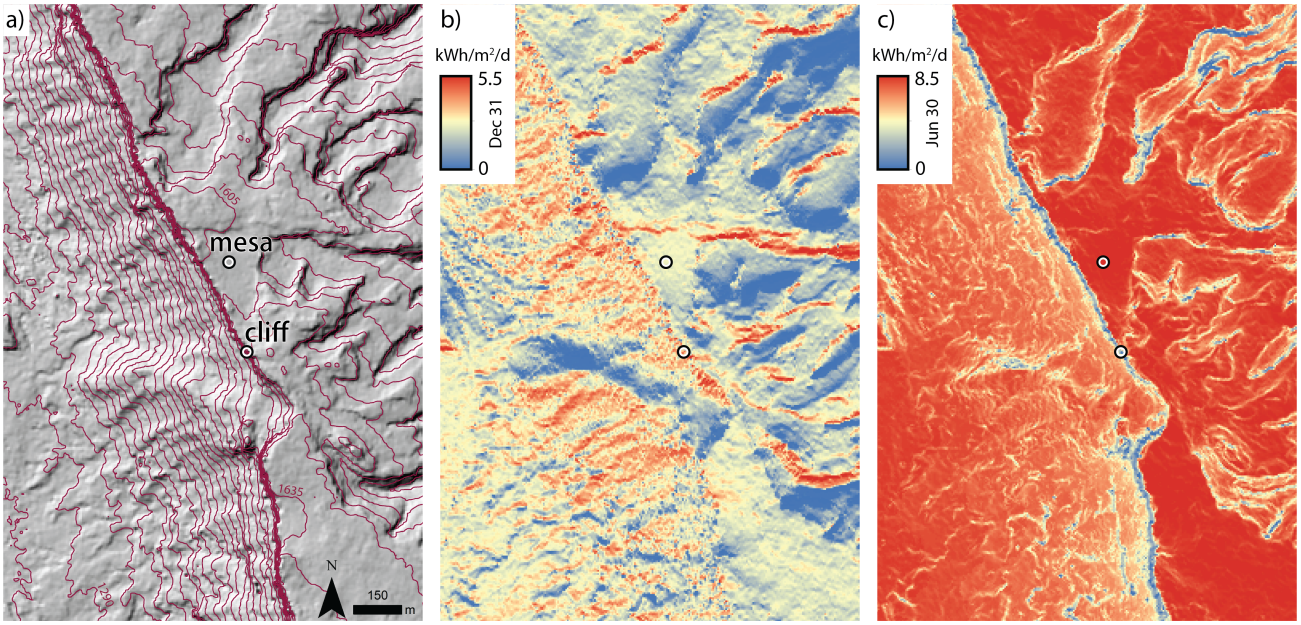

Figure 4 (a) Hillshade of topography with 15 m contour lines at the Kane Springs Ledge study area. Cliff and Mesa monitoring points indicated. (b) Modeled insolation at the end of December, and (c) June.

ness. Modeled daily insolation patterns also compare well with limited in-situ data (Figure 3b), accurately reflecting the timing of sunrise and sunset and capturing the magnitude of daily insolation. Figure 4 shows gridded insolation data for the months of December and June, as well as the locations of the cliff and mesa monitoring points. Comparison of the two months highlights: generally greater insolation in summer, differences between the mesa and cliff sites as well as surrounding areas, and greater insolation on the cliff as compared to the mesa in winter due to lower winter sun angle.

To extend the comparison between annual frequency and insolation trends, we plot mean monthly fundamental frequency (calculated for the end of each month and averaged across the two years) and cumulative insolation modeled for the last day of each month at both the mesa and cliff observation points (Figure 5). Results show similar annual trends between frequency and insolation, and suggest that frequency best correlates with insolation modeled for the upward-facing mesa surface. The west-southwest facing cliff features a notable summer plateau in insolation (Figure 5a), as the higher sun angle means less energy is striking the vertical cliff. This plateau feature is not reflected in frequency monitoring data. Comparing modeled insolation and mean monthly frequency in a scatter plot, we find excellent correlation, which is maximized for model results from the mesa point (Figure 5b). These results affirm our hypothesis that annual resonance frequency drifts at the site are primarily driven by seasonal changes in solar radiation.

Only 14 days of continuous data were available from the onsite pyranometer; however, these measurements show a clear correlation with the timing of daily frequency drifts (Figure 6). In particular, we find that the daily frequency rise is substantially delayed – by about 5 hours – from sunrise and the daily rise in insolation. In

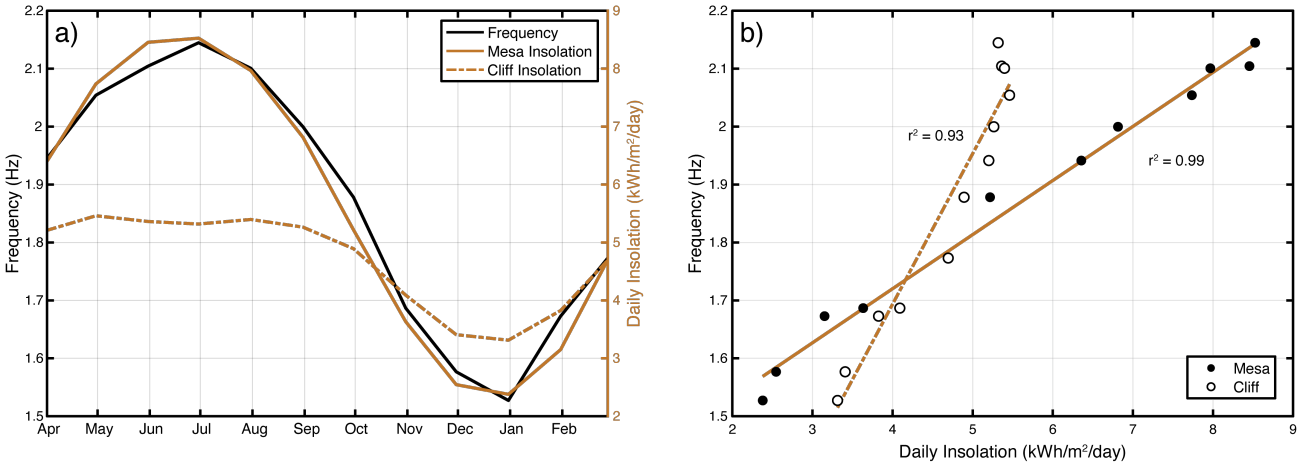

Figure 5 (a) Mean monthly fundamental frequency of Kane Springs Tower shown together with modeled cumulative daily insolation for the mesa and cliff observation points. (b) Mean monthly frequency plotted against insolation for the mesa and cliff sites; linear fits and correlation coefficients shown.

turn, we find that the evening frequency decrease occurs exactly at sunset as insolation drops to zero. We attribute these patterns to the west-facing aspect of the tower: on the daily scale, solar radiation only strikes the cliff starting around noon, many hours after sunrise, and the tower's west face is in full sun throughout the afternoon until insolation is lost at sunset. Coeval data from in-situ air and rock temperature sensors show a daily pattern that differs slightly from frequency and insolation records due to diffusive effects and lag times. For example, rock and air temperatures peak in the afternoon when frequencies are still rising, while the temperature minima are roughly concurrent with sunrise (rock temperature has a minor delay), a time when frequencies are still decreasing. The overnight decrease in frequency closely mimics rock temperature data during this time, reflecting diffusive heat loss from the rock and atmosphere at a time with no incoming solar radiation.

To clarify daily variations beyond the brief period of coeval in-situ climate data, we compare daily trends of modeled insolation with resonance frequency measurements for a representative day at the end of three different months: June, September, and December (Figure 7). Both datasets have 30-min time resolution. While September data are most similar to our in-situ observations, all comparisons show similar trends: frequencies rise each day substantially after sunrise and decrease each day immediately at sunset. The lag time between sunrise and frequency increase is greatest in June and smallest in December, which is also reflected in differences between insolation modeled on the cliff face and mesa top: the lower sun angles in winter means the cliff receives solar radiation earlier in the day as compared to summer. In each case, the timing of resonance frequency drifts best correlates with insolation modeled on the west-southwest facing cliff.

6 Discussion

Resonance frequency data from Kane Springs Tower reveal an interesting annual trend where frequency changes appear to precede air temperature fluctuations. This negative lag time was quantified over our monitoring period as -35 ± 2 days. The value is in contrast to similar datasets in the same region, where frequencies are either in-phase with air temperatures or lag temperature changes by several days or weeks (Geimer et al., 2022; Jensen et al., 2024). Instead, on an annual scale, we find that resonance frequencies are directly correlated and in-phase with insolation. Annual patterns of insolation, in turn, reflect changes in incoming solar radiation created by the Earth's axial tilt, and have minimum and maximum values at the winter and summer solstices, respectively. Insolation is a key component of the Earth's heat budget, driving annual changes in air temperature which has extrema weeks after the solstices. Here we show the importance of solar radiation on annual-scale temperature-frequency relationships, complementing previous findings from daily studies (Guillemot et al., 2022).

Why annual patterns of resonance frequency change at the Kane Springs Tower are in-phase with insolation and not air temperature as at most other monitoring sites is not fully clear. The west-southwest facing aspect of the tower may play a role; however, our annual frequency trends best compare with model results for the upward facing mesa point and not the west-facing cliff. Perhaps more importantly, the tower features a dark patina of desert varnish, which lowers its albedo, making it especially efficient in absorbing solar radiation. Meanwhile, the 3D geometry plays a role in controlling heat transfer, as the heated volume of the tower responsible for driving annual frequency changes is more than skin-deep. If we assume a typical diffusivity for rock of 10^{-6} m^2/s (Jensen et al., 2024), the characteristic length scale for annual changes is $\sim$ 3 m, suggesting that a tower heating and cooling from multiple sides likely experiences full-thickness temperature changes over the year. From these considerations, it appears at our site that the efficiency of heat transfer by radiative effects (insolation) outweighs that from convective effects (air temperature), and thus frequencies best correlate with annual insolation cycles (cf. Guillemot et al., 2024).

We propose that resonance frequency drifts at Kane

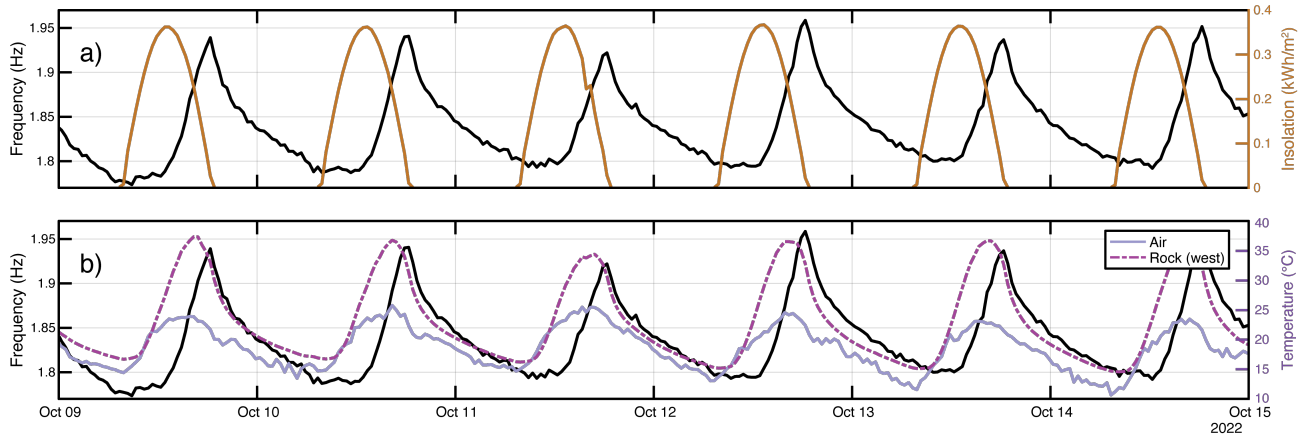

Figure 6 Five days of representative monitoring data from Kane Springs Tower. (a) Fundamental frequency and insolation. Frequency increases each day after sunup with an average delay of ~ 5 hours vs. insolation. Frequencies decrease as insolation reaches zero at sunset. (b) Rock and air temperatures show more complex correlation with frequency and insolation reflecting, in part, lagged diffusive effects. Date markers are at 00:00 MDT.

Springs Tower are caused by material property changes (i.e., stress stiffening) rather than an opening and closing rear crack (Colombero et al., 2021b). The former effect invokes thermoelastic stresses caused by heating and cooling cycles, and a corresponding change in grain contact and microcrack stresses, resulting in material stiffening as the tower warms and softening as the rock cools. From the analytical formulation of a cantilever (e.g. Moore et al., 2019), frequencies are expected to change as $E^{0.5}$, where E is Young's modulus. Therefore, our measured annual resonance frequency change of $\pm$20% (deviation from the mean) relates to an annual variation in Young's modulus of approximately ±10%. This simple relationship, however, assumes uniform material properties, which may be unlikely given the pattern of diffusive heat transfer and corresponding thermal stress propagation in the rock at depth (Geimer et al., 2022). Differences are additionally reflected in the annual amplitudes of $f1$ and $f2$, where the amplitude of $f2$ is $\sim$ 78% that of $f1$, suggesting anisotropic material stiffening which may be related to the different aspects of the tower and the respective mode shapes (Dzubay et al., 2022). Meanwhile, the rear crack at the Kane Springs Tower is too wide for annual thermal expansion of the rock walls to cause changes in crack contact area, which would affect modal mass.

Our approach of using numerical modeling to supplement available in-situ insolation data has several advantages. First, model results overcome our substantial loss of data caused by an unreliable sensor, but more generally, these may also supplement existing data that suffer from gaps or unequal measurement periods. Notably, numerical modeling offers additional flexibility in selecting monitoring points with different orientations, something that would be challenging to manage in field data acquisition, especially on a steep cliff. Modeling annual and daily patterns of insolation is, in turn, not a particularly difficult task for such simulations, as insolation mainly depends on well-established cycles of solar radiation and few local climate variables.

We find clear correlation in the timing of daily insolation and resonance frequency changes through analysis of sparse available data as well as numerical modeling results. Resonance frequencies increase daily as the sun strikes the tower, which is substantially delayed from sunrise due to the west facing aspect. In summer this delay can be more than 5 hours, while it is shorter in winter, an effect related to lower sun angles in winter allowing sunlight to obliquely strike the tower earlier in the morning. Throughout the day, we find that frequencies continue to climb until sunset, despite air and rock temperatures peaking earlier in the afternoon. This pattern again indicates that resonance frequencies, and thus material properties of the tower, vary in relation to insolation cycles on a daily timescale. Meanwhile, the overnight trend of frequency decrease closely mirrors rock temperature changes, reflecting diffusive heat losses from the rock and atmosphere.

An observation facilitated by our insolation model results is the difference between annual and daily correlations between insolation and frequency. We find that annually, frequency values best correlate with insolation modeled for the upward-facing mesa surface, whereas on the daily scale, the timing of frequency changes best correlates with insolation modeled on the west-facing cliff. This difference may be related to the diffusive depth scale for daily and annual changes; whereas the characteristic length for annual changes is $\sim$ 3 m, that for daily changes is $\sim$ 0.16 m, i.e., daily temperature changes only occur in a thin outer skin of the tower while the tower likely heats fully through on an annual scale. The difference might in turn be an artifact of a better correlation coefficient for the annual data with the mesa model results rather than the cliff model results, whereas we see in Figure 5b that both results fit the data reasonably well. Note that the magnitude of daily and annual temperature-related frequency drifts is within the range identified from previous studies, including some in the same area and materials (Geimer et al., 2022; Colombero et al., 2021b) and that while past studies have identified additional inverse correlations between frequency and temperature at subfreezing conditions, our data do reveal evidence of ice-related frequency drifts.

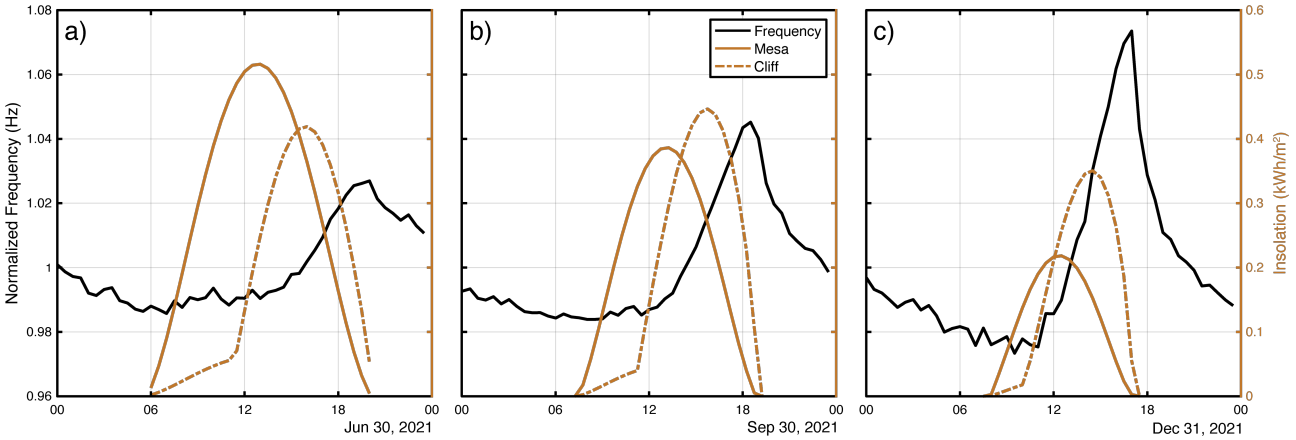

Figure 7 Normalized fundamental frequency for three representative days in (a) June, (b) September, (c) December. For each day, modeled insolation is shown at both the mesa and cliff observation points. June and September times are MDT, December is MST.

Daily frequency drifts also show interesting trends throughout the year. Notably, we find that daily frequency amplitudes are largest in winter and smallest in summer (Figure 7). As more solar radiation strikes the cliff in summer than winter (Figure 5a), we might expect the opposite. Instead, we propose that changing internal stress conditions of the rock mass through the seasons facilitates a greater stress-stiffening response in winter rather than summer (Guillemot et al., 2024). Specifically, lower stresses during winter brought on by thermoelastic contraction cause grain contacts and microcracks to dilate as compared to during summer conditions, and therefore daily wintertime heating can result in a greater change in grain and crack contact stiffness resulting in a larger daily frequency amplitude. In summer, with general warming and higher compressive stresses, microcracks are more closed and daily temperature fluctuations produce less change in the overall rock mass stiffness.

7 Conclusion

We monitored resonance frequencies of a 36-m high sandstone tower in Utah over a period of two years, discovering that frequencies are directly correlated and in phase with annual insolation changes. This is in contrast to most other monitoring datasets, including some from the same area and in similar materials, which show frequencies are in phase with or lag air temperature changes by days to weeks. We attribute frequency changes at the tower to material stiffness changes during heating and cooling, rather than rear crack aperture changes, as the bounding crack is too wide to close during summer warming. We hypothesize that the dark patina of desert varnish on many parts of the tower's steep faces lowers the rock albedo and facilitates efficient transfer of solar radiation, making the feature particularly sensitive to insolation. This hypothesis is supported by patterns of daily resonance frequency drifts at the site which show an increase several hours after sunrise, as sun strikes the west-southwest facing tower cliff face, and a daily frequency decrease at sundown. Our dataset is one of only a few cases of long-term resonance frequency monitoring reported in the literature. As the technique becomes increasingly applied for slope stability analysis and structural health monitoring, it is crucial to understand factors that influence reversible frequency drifts if these are to be accounted for in damage detection algorithms. Here we established that resonance frequencies of Kane Springs Tower are correlated with annual changes in insolation, rather than air temperature, as observed at most other sites. The outcome is that lag times between frequency and (the more easily-measured) temperature can be both positive (normally observed) and negative (our observations). Our results indicate that substantial resonance frequency data may be needed in establishing a slope instability monitoring site to support damage detection in the presence of large environmentally driven drifts.

Acknowledgements

We are grateful to the field assistants that made this research possible over several years: Oliver Moore, Riley Finnegan, Molly McCreary, Tessa Czech, Adam Smith, and Madeleine Festin. Many thanks to Sebastiano D'Amico and an anonymous reviewer for helpful and collegial feedback during the review process. This material is based upon work supported by the National Science Foundation under Award No. 2150896. Any opinions, findings and conclusions or recommendations expressed in this material are those of the author(s) and do not necessarily reflect the views of the National Science Foundation.

Data and code availability

Seismic data generated in this study are available at https://doi.org/10.7914/SN/5P_2013.

Competing interests

The authors declare no competing interests.

References

Anthony, R. E., Ringler, A. T., Wilson, D. C., and Wolin, E. Do low-cost seismographs perform well enough for your network? An overview of laboratory tests and field observations of the OSOP Raspberry Shake 4D. *Seismological Research Letters*, 90 (1):219–228, 2019. doi: https://doi.org/10.1785/0220180251.

Arosio, D., Aguzzoli, A., Zanzi, L., Panzeri, L., and Scaccabarozzi, D. Lab and Field Tests of a Low-Cost 3-Component Seismometer for Shallow Passive Seismic Applications. *Earth and Space Science*, 10(10):e2023EA002934, 2023. doi: 10.1029/2023EA002934.

Bessette-Kirton, E. K., Moore, J. R., Geimer, P. R., Finnegan, R., Häusler, M., and Dzubay, A. Structural characterization of a toppling rock slab from array-based ambient vibration measurements and numerical modal analysis. *Journal of Geophysical Research: Earth Surface*, 127(8):e2022JF006679, 2022. doi: 10.1029/2022JF006679.

Bottelin, P., Jongmans, D., Baillet, L., Lebourg, T., Hantz, D., Lévy, C., Le Roux, O., Cadet, H., Lorier, L., Rouiller, J.-D., et al. Spectral analysis of prone-to-fall rock compartments using ambient vibrations. *Journal of Environmental and Engineering Geophysics*, 18(4):205–217, 2013a. doi: 10.2113/JEEG18.4.205.

Bottelin, P., Levy, C., Baillet, L., Jongmans, D., and Gueguen, P. Modal and thermal analysis of Les Arches unstable rock column (Vercors massif, French Alps). *Geophysical Journal International*, 194(2):849–858, 2013b. doi: 10.1093/gji/ggt046.

Bottelin, P., Baillet, L., Larose, E., Jongmans, D., Hantz, D., Brenguier, O., Cadet, H., and Helmstetter, A. Monitoring rock reinforcement works with ambient vibrations: La Bourne case study (Vercors, France). *Engineering Geology*, 226:136–145, 2017. doi: 10.1016/j.enggeo.2017.06.002.

Bottelin, P., Baillet, L., Carrier, A., Larose, E., Jongmans, D., Brenguier, O., and Cadet, H. Toward workable and cost-efficient monitoring of unstable rock compartments with ambient noise. *Geosciences*, 11(6):242, 2021. doi: 10.3390/geosciences11060242.

Burjánek, J., Gassner-Stamm, G., Poggi, V., Moore, J. R., and Fäh, D. Ambient vibration analysis of an unstable mountain slope. *Geophysical Journal International*, 180(2):820–828, 2010. doi: 10.1111/j.1365-246X.2009.04451.x.

Burjánek, J., Moore, J. R., Yugsi Molina, F. X., and Fäh, D. Instrumental evidence of normal mode rock slope vibration. *Geophysical Journal International*, 188(2):559–569, 2012. doi: 10.1111/j.1365-246X.2011.05272.x.

Burjánek, J., Gischig, V., Moore, J. R., and Fäh, D. Ambient vibration characterization and monitoring of a rock slope close to collapse. *Geophysical Journal International*, 212(1):297–310, 2018. doi: DOI: 10.1093/gji/ggx424.

Cole Jr, H. A. On-line failure detection and damping measurement of aerospace structures by random decrement signatures. Technical report, NASA, 1973.

Colombero, C., Baillet, L., Comina, C., Jongmans, D., and Vinciguerra, S. Characterization of the 3-D fracture setting of an unstable rock mass: From surface and seismic investigations to numerical modeling. *Journal of Geophysical Research: Solid Earth*, 122(8):6346–6366, 2017. doi: 10.1002/2017JB014111.

Colombero, C., Godio, A., and Jongmans, D. Ambient seismic noise and microseismicity monitoring of a prone-to-fall quartzite tower (Ormea, NW Italy). *Remote Sensing*, 13(9):1664, 2021a. doi: 10.3390/rs13091664.

Colombero, C., Jongmans, D., Fiolleau, S., Valentin, J., Baillet, L., and Bièvre, G. Seismic noise parameters as indicators of reversible modifications in slope stability: a review. *Surveys in Geophysics*, 42:339–375, 2021b. doi: 10.1007/s10712-021-09632-w.

Corripio, J. G. Vectorial algebra algorithms for calculating terrain parameters from DEMs and solar radiation modelling in mountainous terrain. *International Journal of Geographical Information Science*, 17(1):1–23, 2003. doi: 10.1080/713811744.

Del Gaudio, V. and Wasowski, J. Advances and problems in understanding the seismic response of potentially unstable slopes. *Engineering geology*, 122(1-2):73–83, 2011. doi: 10.1016/j.enggeo.2010.09.007.

Del Gaudio, V., Wasowski, J., and Muscillo, S. New developments in ambient noise analysis to characterise the seismic response of landslide-prone slopes. *Natural hazards and earth system sciences*, 13(8):2075–2087, 2013. doi: 10.5194/nhessd-1-1319-2013.

Dzubay, A., Moore, J. R., Finnegan, R., Jensen, E. K., Geimer, P. R., and Koper, K. D. Rotational Components of Normal Modes Measured at a Natural Sandstone Tower (Kane Springs Canyon, Utah, USA). *The Seismic Record*, 2(4):260–268, 2022. doi: 10.1785/0320220035.

Finzi, Y., Ganz, N., Dor, O., Davis, M., Volk, O., Langer, S., Arrowsmith, R., and Tsesarsky, M. Stability analysis of fragile rock pillars and insights on fault activity in the Negev, Israel. *Journal of Geophysical Research: Solid Earth*, 125(12):e2019JB019269, 2020. doi: 10.1029/2019JB019269.

Fiolleau, S., Jongmans, D., Bièvre, G., Chambon, G., Baillet, L., and Vial, B. Seismic characterization of a clay-block rupture in Harmalière landslide, French Western Alps. *Geophysical Journal International*, 221(3):1777–1788, 2020. doi: 10.1093/gji/ggaa050.

Geimer, P. R., Finnegan, R., and Moore, J. R. Meteorological controls on reversible resonance changes in natural rock arches. *Journal of Geophysical Research: Earth Surface*, 127(10): e2022JF006734, 2022. doi: 10.1029/2022JF006734.

Guillemot, A., Baillet, L., Larose, E., and Bottelin, P. Changes in resonance frequency of rock columns due to thermoelastic effects on a daily scale: observations, modelling and insights to improve monitoring systems. *Geophysical Journal International*, 231(2):894–906, 2022. doi: 10.1093/gji/ggac216.

Guillemot, A., Audin, L., Larose, É., Baillet, L., Guéguen, P., Jaillet, S., and Delannoy, J.-J. A comprehensive seismic monitoring of the pillar threatening the world cultural heritage site Chauvet-Pont d'Arc cave, toward rock damage assessment. *Earth and Space Science*, 11(4):e2023EA003329, 2024. doi: 10.1029/2023EA003329.

Häusler, M., Michel, C., Burjánek, J., and Fäh, D. Fracture network imaging on rock slope instabilities using resonance mode analysis. *Geophysical Research Letters*, 46(12):6497–6506, 2019.

Häusler, M., Michel, C., Burjanek, J., and Fäh, D. Monitoring the Preonzo rock slope instability using resonance mode analysis. *Journal of Geophysical Research: Earth Surface*, 126(4): e2020JF005709, 2021. doi: 10.1029/2020JF005709.

Ibrahim, S. Random decrement technique for modal identification of structures. *Journal of Spacecraft and Rockets*, 14(11): 696–700, 1977. doi: 10.2514/3.57251.

Jensen, E. and Moore, J. Coevolution of rock slope instability damage and resonance frequencies from distinct-element modeling. *Journal of Geophysical Research: Earth Surface*, 128(11): e2023JF007305, 2023. doi: 10.1029/2023JF007305.

Jensen, E. K., Moore, J. R., Geimer, P. R., and Finnegan, R. Combined ambient vibration and surface displacement measurements for improved progressive failure monitoring at a toppling rock slab in Utah, USA. *Frontiers in Earth Science*, 12:1364653, 2024. doi: 10.3389/feart.2024.1364653.

Jongmans, D., Baillet, L., Larose, E., Bottelin, P., Mainsant, G., Chambon, G., and Jaboyedoff, M. Application of ambient vibration techniques for monitoring the triggering of rapid landslides. In *Engineering Geology for Society and Territory-Volume 2: Landslide Processes*, pages 371–374. Springer, 2015.

Kleinbrod, U., Burjánek, J., and Fäh, D. Ambient vibration classification of unstable rock slopes: A systematic approach. *Engineering Geology*, 249:198–217, 2019. doi: 10.1016/j.enggeo.2018.12.012.

Koper, K. D. and Burlacu, R. The fine structure of double-frequency microseisms recorded by seismometers in North America. *Journal of Geophysical Research: Solid Earth*, 120(3):1677–1691, 2015. doi: 10.1002/2014JB011820.

Kumar, L., Skidmore, A. K., and Knowles, E. Modelling topographic variation in solar radiation in a GIS environment. *International journal of geographical information science*, 11(5): 475–497, 1997. doi: 10.1080/136588197242266.

Lévy, C., Baillet, L., Jongmans, D., Mourot, P., and Hantz, D. Dynamic response of the Chamousset rock column (Western Alps, France). *Journal of Geophysical Research: Earth Surface*, 115 (F4), 2010. doi: https://doi.org/10.1029/2009JF001606.

Moore, J. R., Gischig, V., Burjanek, J., Loew, S., and Fäh, D. Site effects in unstable rock slopes: dynamic behavior of the Randa instability (Switzerland). *Bulletin of the Seismological Society of America*, 101(6):3110–3116, 2011. doi: 10.1785/0120110127.

Moore, J. R., Geimer, P. R., Finnegan, R., and Michel, C. Dynamic analysis of a large freestanding rock tower (Castleton Tower, Utah). *Bulletin of the Seismological Society of America*, 109(5): 2125–2131, 2019. doi: 10.1785/0120190118.

Müller, J. and Burjánek, J. In situ estimation of effective rock elastic moduli by seismic ambient vibrations. *International Journal of Rock Mechanics and Mining Sciences*, 170:105459, 2023. doi: 10.1016/j.ijrmms.2023.105459.

Pilz, M., Parolai, S., Bindi, D., Saponaro, A., and Abdybachaev, U. Combining seismic noise techniques for landslide characterization. *Pure and Applied Geophysics*, 171:1729–1745, 2014. doi: 10.1007/s00024-013-0733-3.

Plummer, M. A. and Phillips, F. M. A 2-D numerical model of snow/ice energy balance and ice flow for paleoclimatic interpretation of glacial geomorphic features. *Quaternary Science Reviews*, 22(14):1389–1406, 2003. doi: 10.1016/S0277-3791(03)00081-7.

Starr, A. M., Moore, J. R., and Thorne, M. S. Ambient resonance of Mesa Arch, Canyonlands National Park, Utah. *Geophysical Research Letters*, 42(16):6696–6702, 2015. doi: 10.1002/2015GL064917.

Taruselli, M., Arosio, D., Longoni, L., Papini, M., and Zanzi, L. Seismic noise monitoring of a small rock block collapse test. *Geophysical Journal International*, 224(1):207–215, 2021. doi: 10.1093/gji/ggaa447.

Valentin, J., Capron, A., Jongmans, D., Baillet, L., Bottelin, P., Donze, F., Larose, E., and Mangeney, A. The dynamic response of prone-to-fall columns to ambient vibrations: comparison between measurements and numerical modelling. *Geophysical Journal International*, 208(2):1058–1076, 2017. doi: 10.1093/gji/ggw440.